Available online at www.sciencedirect.com

ScienceDirect

Procedia Structural Integrity 38 (2022) 300–308

Structural Integrity Procedia

www.elsevier.com/locate/procedia

FATIGUE DESIGN 2021, 9th Edition of the International Conference on Fatigue Design

Determination of fatigue crack propagation thresholds using small-scale specimens

Tiago Werner[a,*], Sergio Blasón[a], Mauro Madia[a], Julius Kruse[a], Matteo Benedetti[b]

[a]*Bundesanstalt für Materialforschung und -prüfung (BAM), Unter den Eichen 87, 12205 Berlin, Germany*
[b]*University of Trento, Department of Industrial Engineering, via Sommarive 9, 38123 Povo, Italy*

Abstract

The damage tolerance approach is widely used in the design and estimation of inspection intervals of safety-relevant metallic components subject to fatigue loading. The approach relies on the knowledge of the fatigue crack propagation characteristics, wherein a relevant role is played by the fatigue crack propagation threshold. Nevertheless, the use of material data determined by testing on conventional specimens is not straightforward in the case of thin-walled components such as turbine blades or additively manufactured parts, in which the local variation of material properties in highly stressed regions must be considered. In these cases, the possibility of investigating the fatigue crack propagation properties on a limited portion of material is crucial. For this purpose, a new test procedure has been developed for small-scale specimens which allows the determination of the intrinsic fatigue crack propagation threshold and the near-threshold regime. The validity and limitations of the method are demonstrated on the high strength steel S960QL, along with a comparison with data determined by testing on conventional geometries.

Keywords: fatigue crack propagation threshold; small-scale specimens; high strength steel; crack-tip constraint; damage tolerance

* Corresponding author. Tel.: +49-30-81043146; fax: +49-30-810431467.
E-mail address: Tiago.Werner@bam.de

10.1016/j.prostr.2022.03.031

1. Introduction

The highest percentage of component life under fatigue loading conditions is spent during the development of short cracks and the initial phase of long cracks. The use of Fracture Mechanics for the characterization of fatigue crack growth rate (FCGR) curves has proven to be a useful and adequate tool in the prediction of fatigue lifetimes provided that certain conditions are satisfied. All of the above implies the need to have a methodical and accurate evaluation procedure of the response of the material to be studied to achieve a reliable prediction of the lifetime of components under safe conditions, based on the damage tolerance approach. Only in this way a proper design and assessment in terms of structural integrity are possible, including the definition of inspection intervals.

Meanwhile, the optimization of designs supported by technological development means that over time the thicknesses of components subjected to high mechanical stress show increasing differences concerning those commonly studied and defined in standards and design guidelines, as well as the experimental studies that can be found in the literature nowadays. Examples of thin-walled components are turbine blades or certain additively manufactured parts where, in addition, variations in material properties can occur locally which should also be analyzed. This emphasizes the necessity to investigate the mechanical behavior in specimens with decreasing sizes and the consideration of possible size-related effects.

Also, the possibility of extracting small specimens directly on in-service components is an important aspect to contemplate. The implementation of non-invasive analysis techniques allows the study of the material's response in locations that, once the stress conditions are known, are likely to lead to the loss of minimum safety requirements and structural integrity. The Small Punch Test (SPT) is an example of an experimental technique that can be classified as non-destructive (NDT), although its scope of application is currently limited mainly to the characterization of static stresses. In this regard, the use of miniature specimens for the study of behavior under fatigue loading is considered to be a developing field of research with a wide margin for exploration, see Murchio et al. (2021).

Consequently, this work arises from the approach of a hypothetical change in the response of the material when confronting its performance between significantly different specimen thicknesses and controlled laboratory conditions. The experimental determination of the intrinsic threshold value and, in general, characterization of FCGR curves on S960QL high strength steel is presented using specimens of similar geometry, although with different sizes. In all cases, the analysis is carried out in the long crack regime. At the same time, predominantly elastic-linear conditions are accepted to be valid during all the tests, so that the crack driving force can be expressed in terms of the stress intensity factor range.

Finally, the main features of the experimental procedure are described in detail, and certain differences concerning the recommendations defined in the reference standards are discussed, along with the main limitations to be taken into account when carrying out this type of testing.

Nomenclature

α_g	global constraint factor
ΔF	force range
ΔK	stress intensity factor range
ΔK_{eff}	effective stress intensity factor range
ΔK_{th}	threshold value of the stress intensity factor range
$\Delta K_{th,eff}$	intrinsic threshold
$\Delta K_{th,op}$	opening stress intensity factor range; extrinsic part of the threshold
ε	strain
λ	Parameter for the determination of the minimum un-cracked ligament according to ISO12108
σ	stress
$\sigma_{I,m}$	Finite element modelling: mode I opening stress acting on A_m
a; a_0	crack size; initial crack size
A_m	Finite element modeling: projected area of a yielded element m on the uncracked ligament
A_T	Finite element modeling: total projected area for all yielded elements on the uncracked ligament
B	specimen thickness

C	normalized K-gradient, $C = 1/K \cdot dK/da$
COD	crack opening displacement
da/dN	crack propagation rate
DCPD	direct current potential drop
E	young's modulus
EDM	electrical discharge machining
F_{max}	force peak value during cyclic loading under ΔF=cte conditions
K'	cyclic strain hardening coefficient
K_{max}	maximum stress intensity factor
R	load ratio
$R_{p0.2}$	material yield strength
SEN B	Single Edge Notch Bend specimens
n'	cyclic strain hardening exponent
V; V_0	electric potential; initial electric potential
W	specimen width
y	distance between the crack plane and each of the contact probes in the DCPD monitoring system

2. Experimental procedure

2.1. Range of application

The study presented here is limited to the long crack regime and it aims at identifying the intrinsic value ($\Delta K_{th,eff}$) and near-threshold regime of the high-strength steel S960QL. For this purpose, the load ratio (R) applied in all tests was 0.8. In line with several preliminary studies, it is considered that the full range of the stress intensity factor (ΔK) can be considered effective for values of $R \geq 0.8$, such that the crack is accepted to be entirely opened over the whole ΔK range. Conversely, at $R < 0.8$, the estimation of ΔK_{th} must take into account crack closure effects, whereby $\Delta K_{th} = \Delta K_{th,eff} + \Delta K_{th,op}$. Nevertheless, certain crack closure effects in the vicinity of ΔK_{th} can be detected even at the relatively high value of the load ratio tested (R = 0.8), probably due to oxidation effects. However, they have no practical significance in the estimation of the threshold values, and that is why they are not investigated in this work.

2.2. Determination of the intrinsic threshold $\Delta K_{th,eff}$ and near-threshold regime

The loading conditions in terms of force both for the estimation of ΔK_{th} and in the description of the lower span of the FCGR curves remained constant throughout the entire test, i.e. ΔF=constant. This is opposed to the recommendations of ISO 12108 and ASTM 647, the two reference standards usually considered in this regard. Both suggest the K-decreasing procedure in the study of da/dN rate values below 10^{-5} mm/cycle. However, they warn about the influence that the normalized K-gradient, denoted in both standards as $C = 1/K \cdot dK/da$, may have on the results, leaving the responsibility for the analysis of its sensitivity to the user. Other test procedures for the determination of ΔK_{th} are feasible and some studies analyze the differences between them, see Newman and Yamada (2010).

Thus, once the pre-cracking phase has been completed, the test proceeds by looking for the value of ΔF that triggers continuous crack propagation. The methodology necessarily involves some initial exploration, with small gradual ΔF increments when no crack extension is detected after a fixed number of cycles, similar to that proposed by Tabernig and Pippan (2002). Since the applied ΔK is fully effective to crack propagation given the high applied R, no crack arrest due to the accumulation of closure effects would be expected.

It is therefore recognized that the sensitivity of the procedure in the determination of ΔK_{th} is partly conditioned by the magnitude of the successive incremental steps until reaching a value of ΔK such that propagation onset is achieved. In this study, 0.1 MPa·m$^{1/2}$ was set as the incremental step. In any case, the ΔK_{th} is not determined as the ΔK value at which the crack starts propagating, but it is rather identified according to the criteria defined in the referred standards (extrapolated at 10^{-8} mm/cycle according to ISO 12108).

2.3. Experimental setup

The study has been conducted using single etch notched specimens in bending load (SEN B), comparing different geometries, distinguishing between "*conventional*" and "*miniature*" ones. The former ones have been machined with a thickness (B) of 6 mm and width (W) of 19 mm. The reduced scale specimens analyzed in this work had a thickness of 3 mm and two different widths, 4 and 6 mm.

The conventional specimens have been machined with a straight notch, subsequently sharpened using a razor blade. To minimize asymmetrical crack propagation, chevron notches have been used in case of small-scale specimens. These are characterized by an angle of 150° as in Kovarik et al. (2017) and have been produced by electrical discharge machining (EDM).

The 4-point and 8-point bending test fixtures have been used to test conventional geometry specimens. The miniature specimens have been tested in the 3-point and 4-point bending fixtures. Figure 1 shows the SEN B8 and SEN B3 experimental setup.

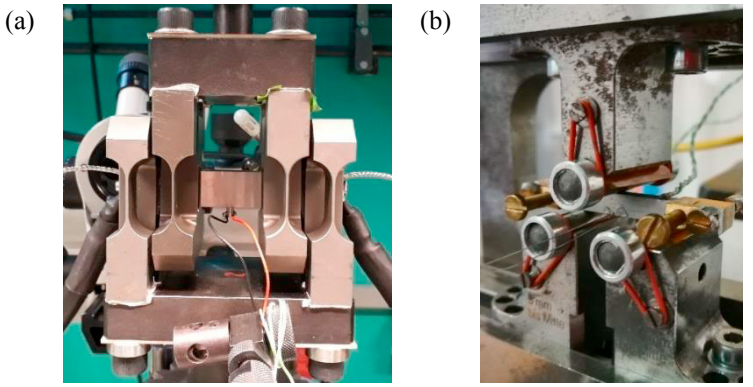

Fig. 1. Experimental setup: (a) SEN B8 (19x6 mm specimen); (b) SEN B3 (4x3 mm specimen).

The conventional specimens were tested on a RUMUL resonant fatigue testing machine with 100 kN load capacity. In contrast, the miniature specimens were tested on a Schenck servo-hydraulic universal testing machine with a 10 kN load cell and MTS control system.

2.4. Crack length monitoring

The direct current potential drop (DCPD) technique has been used for crack size monitoring throughout all tests. Thus, the crack length monitoring is related to the potential drop, V, according to Johnson (1965) following Eq. (1), where the initial crack size and electrical potential are denoted as a_0 and V_0, respectively; the variable y symbolizes the distance between the crack plane and each of the contact probes on either side of it. Compensation for temperature effects on the material resistivity has been also implemented.

$$\frac{a}{W} = \frac{2}{\pi}\cos^{-1}\left\{\frac{\cosh\left(\frac{\pi y}{2W}\right)}{\cosh\left(\frac{V}{V_0}\cosh^{-1}\left[\frac{\cosh\left(\frac{\pi y}{2W}\right)}{\cos\left(\frac{\pi a_0}{2W}\right)}\right]\right)}\right\} \tag{1}$$

The pre-cracking phase has been conducted under R = 0.1, gradually reducing the load in 4 stages keeping ΔF constant, ensuring that at the end of this stage the K_{max} value did not exceed the value initially foreseen at the beginning of the propagation test with R = 0.8. The size of the pre-crack in the reduced specimens has been generally limited to

1 mm extension, although this did not comply with the recommendation of the standards. According to the prescriptions in the standards, a minimum pre-crack corresponding to the sum of the notch length and an additional 1 mm should have been produced in order to avoid any influence that the shape of the crack front or the loading history during pre-cracking might have on the calibration of the analytical expressions defining the K value. The two main reasons for refuting this requirement were a) to have a sufficiently large range of experimental values to compare results throughout about two orders of magnitude in terms of da/dN, and b) to avoid an excessively small value of the force amplitude during testing that would lead to anomalies or inaccuracies in the machine's performance.

It should be noted that, during the miniature specimen tests, the maximum load amplitude value was in all cases below 200 N, even as low as 37 N. Therefore, maintaining a moderate variation in the F_{max} values during each test was a challenge when working with a servo-hydraulic machine with 10 kN load capacity. Nevertheless, it was always possible to keep the force peak values around ±1% of the nominal applied value, which conforms well to the demands of the standards (±2%).

The fracture surface in each test has been analyzed using a Keyence VHX-2000 optical microscope. In fact, the value of a_0 in Eq. (1) can be measured only at the surface before starting the test. Therefore, a post-mortem analysis of the specimens under the microscope is necessary to correct the a_0 value originally evaluated. Likewise, the average value of the crack size at the end of the test is determined as well. Based on these optical measurements, the value of y in Eq. (1) can be optimized and the crack length values corrected over the entire crack propagation range. Figure 2 shows an example of a result when correction is evaluated in terms of crack size versus the number of cycles.

Although the deviations when corrections are completed are generally not significant, it is a good practice to minimize any source of uncertainty other than that arising from the inherent scatter in the material response. When such a correction is applied, the driving force values will increase or decrease slightly, depending on the direction of the compensation.

In addition, the small effects of minimal misalignments (≤ 200 μm) between the top roller and the crack plane in the case of the SEN B3 configuration, which are unavoidable, were also taken into account.

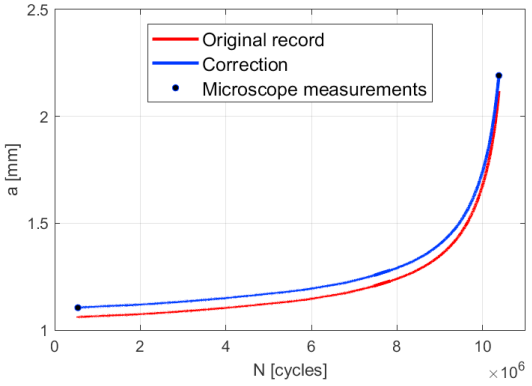

Fig. 2. Example of crack length correction.

3. Experimental results

Each test has been extended to the limit that would allow large-scale yielding effects to be avoided. This limit is defined by the test configuration and the material yield strength ($R_{p0.2}$), where 960 MPa is the characteristic value for the steel under investigation. Eq. (2) establishes the maximum crack size for the validity of the linear elastic ΔK as a driving force in the case of bending specimens (according to ISO 12108). The λ-value is dependent on the distance between supports of each test configuration.

$$a \leq W - \left(\frac{3 \cdot \lambda \cdot F_{max}}{2 \cdot B \cdot R_{p0,2}} \right)^{1/2} \tag{2}$$

In the case of the conventional geometry specimens, previous experimental results were already available to confirm the optimal performance of the measuring and control devices. An initial beach-marking test has been carried out before the experimental campaign on the miniature specimens. The objective of this first test was to verify that the calibration and operating parameters of all the instrumentation were correct. The test has been carried out by alternating R-values of 0.1 and 0.7, with crack increments of 0.3 and 0.1 mm, respectively. Fig. 3(a) shows the fractography of this first calibration test.

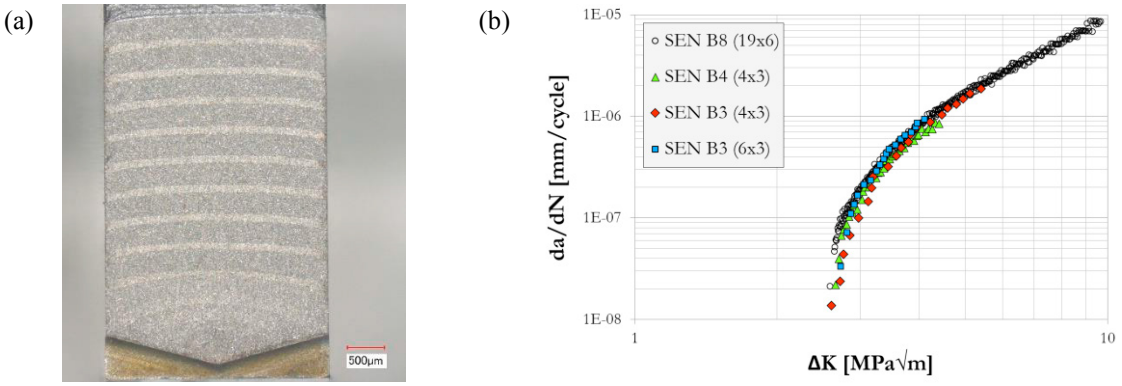

Fig. 3. Crack propagation tests: (a) beach-marking test (6x3 mm specimen); (b) FCGR curves results.

Figure 3(b) shows a selection of the results obtained. The values of ΔK at which the onset of propagation occurred in each test vary in the range 2.5-2.7 MPa·m$^{1/2}$. It must be noted that only data in the near-threshold regime could be collected in case of small-scale specimens, as the maximum ΔK which could be reached during the tests was slightly above 5 MPa·m$^{1/2}$.

Figure 4 shows two examples of the resulting fracture surface on specimens of reduced geometry (W equal to 4 mm and 6 mm, respectively). In both cases, the transition mark between the pre-crack and the propagation itself is well defined. This holds true also for the final crack size. Furthermore, symmetric evolution of the crack, favored by the chevron notch, is evident.

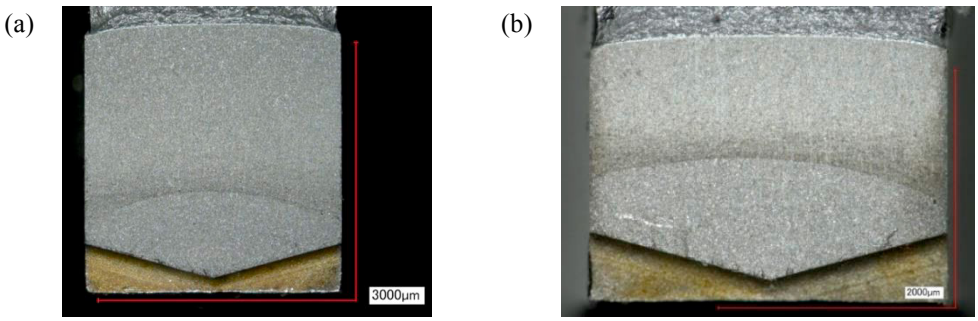

Fig. 4. Fracture surfaces: (a) SEN B3 (6x3 mm specimen); (b) SEN B3 (4x3 mm specimen).

4. Numerical characterization of the crack-tip constraint

The comparison of the fatigue crack propagation characteristics depicted in Fig. 3(b) shows a discrepancy between the data obtained on small-scale specimens when compared to the conventional geometry tested. In particular, small-scale specimens show a slightly lower fatigue crack propagation rate in the near-threshold regime. Even though the difference could be regarded as negligible and the values of $\Delta K_{\mathrm{th,eff}}$ belonging to a single scatter band, it has been decided to investigate the crack-tip stress state in both specimen configurations in the attempt to interpret the experimental outcomes better.

Finite element models have been built up considering the geometries and boundary conditions employed in the experimental tests. Due to the double symmetry given by the longitudinal plane and crack plane, only one-fourth of the specimen has been modelled. To the aim of having a thorough description of the stress field ahead of the crack-tip, the mesh has been extremely refined in this region. In general, the extension of the plastic region has been considered and at least 10 elements have been arranged in the radial direction within the plastic zone. Quadratic isoparametric elements with reduced integration have been used (C3D20R in the general-purpose finite element code Abaqus). The stabilized cyclic stress-strain characteristic of the material has been considered and modelled according to the Ramberg-Osgood relationship

$$\varepsilon = \frac{\sigma}{E} + \left(\frac{\sigma}{K'}\right)^{\frac{1}{n'}}. \tag{3}$$

The young's modulus E = 210 GPa, the cyclic strain hardening coefficient K' = 1367 MPa, and the cyclic strain hardening exponent n' = 0.089 for the S960QL in Eq. (3) have been already published in Kucharczyk et al. (2018).

The global constraint factor (α_g) introduced by Newman et al. (1993) has been used as measure of the crack-tip constraint:

$$\alpha_g = \frac{1}{A_T} \cdot \sum_{m=1}^{M} \left(\frac{\sigma_{I,m}}{\sigma_0}\right) \cdot A_m \tag{4}$$

where A_m is the projected area on the uncracked ligament of a yielded element m in the plastic region, $\sigma_{I,m}$ the mode I opening stress acting on A_m, σ_0 is the yield strength and A_T is the total projected area for all yielded elements (extension of the plastic region on the uncracked ligament). Note that σ_0 has been taken as the 0.2% yield offset of the stabilized cyclic response (786 MPa for the S960QL). The crack-tip constraint for conventional and small-scale specimens has been compared taking into account the same applied mode I stress intensity factor. By doing this, the only difference in the crack-tip stress field is related to the crack-tip constraint. The results of the comparison are reported in Fig. 5. It results clearly that the conventional specimen shows a higher constraint for every simulated load level. The possible outcome in view of the interpretation of the fatigue crack propagation data will be given in the discussion.

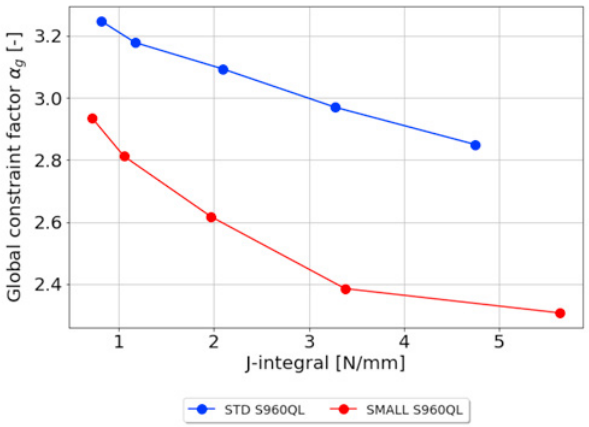

Fig. 5. Comparison of the global constraint factors for different applied loads (expressed in terms of J-integral).

5. Discussion

5.1. Characterization of the fatigue crack propagation behavior

A satisfactory agreement between the tests under different configurations can be established given the results. Despite the dispersion between the curves is within the usual range for the fatigue response of steels with similar properties, small-scale specimens show higher fatigue crack propagation thresholds systematically.

Regarding the determination of ΔK_{th} values, it should be noted that the definition criterion varies, arbitrarily, depending on whether the standard ISO 12108 or ASTM E647 is considered. There are other proposals, in the authors' opinion more reasonable, that allow a back-extrapolation of the experimental values to deduce the threshold values more consistently, together with a complete evaluation of the FCGR curve. Such is the case of the original proposal by Castillo and Canteli (2014), whose advantages of application compared to the most recurrent models today, as well as its capability of developing evaluations under different load-R conditions, are analysed in detail by Blasón (2019).

The finite element simulations offered a further interpretation of the near-threshold data based on the evaluation of the crack-tip constraint. The higher constraint found in the conventional specimen would lead to a higher mode I opening stress ahead of the crack-tip, given the same applied stress intensity factor. This could explain the systematic lower intrinsic crack propagation threshold found during the tests on conventional specimens compared to small-scale ones. Another possible point of view would be related to the phenomenon of plasticity-induced crack closure. Despite the high-stress ratio ($R = 0.8$), it could have a very limited influence on the crack driving force. The lower constraint in the small-scale specimens generates a larger plastic region which would remain as a plastic wake for a growing crack, therefore inducing a slightly higher crack closure which would justify the higher fatigue crack propagation threshold. Nevertheless, these are speculations that need to be confirmed by further analyses.

5.2. Limitations

The experimental campaign carried out identified a series of limitations regarding the use of small specimens for the characterisation of crack propagation rate. These restrictions are mostly related to the maximum admissible ligament to ensure essentially linear elastic conditions, namely:

a) *Sensitivity of the measurement technique*: it is essential to have crack size monitoring devices capable of detecting the advance of a few microns, otherwise the region in the vicinity of the ΔK_{th} threshold could not be characterised. According to the authors' experience and their knowledge of the features of other recording methods (crack gages, COD-compliance, optical microscopy), the technique based on the electric potential drop is currently the most recommendable one as it allows sensitivities below 10 μm, as opposed to the others that can possibly only reach resolutions above 100 μm. At the same time, it should be noted that optical methods are not recommended for this purpose, as they only allow the crack advance to be controlled superficially.

b) *Admissible yield stress*: reproducing this type of analysis only seems feasible for materials with relatively high yield stress. Unless this is the case, the admissible crack propagation under elastic conditions would be very small.

c) *Load ratio*: the occurrence of crack closure effects at small R values requires significantly larger crack extensions to reach the long-crack regime compared to the exposed case of $R = 0.8$, where it can be assumed that the whole ΔK range is effective.

d) *K-Decreasing*: Compared to the practice based on ΔF-constant conditions, the variant developed according to decreasing values of ΔK makes its implementatiwon complicated because it requires larger crack extensions to reach values close to ΔK_{th}.

e) *Measurable ΔK range*: all the above observations highlight the difficulty of describing the crack propagation behavior beyond the area commonly identified as the near-threshold regime. Therefore, it is practically unfeasible to use a single specimen to obtain values of the threshold zone and the Paris region at the same time.

The sensitivity requirements of the load application equipment also deserve special attention. The small dimensions of the specimens require an optimal calibration of the control systems of the machines to reduce the variations of the force peaks within acceptable margins.

6. Conclusions

The evaluation of the experimental results confirms the good agreement between the different geometries and test configurations used, as well as the feasibility of using small-scale specimens in the characterisation of the intrinsic threshold value ($\Delta K_{th,eff}$) of the material and the initial region of the FCGR curves. This opens new perspectives regarding the use of small-scale specimens in the characterisation of materials under fatigue and, particularly, on the study of the response by extracting samples directly from components in service.

The experimental campaign carried out allows to provide recommendations to successfully reproduce similar tests using small specimens on steel and, foreseeably, on other metallic materials.

There are several limitations to consider before embarking on an experimental campaign based on small-scale specimens. The main factor to be considered is the maximum admissible ligament to ensure essentially elastic conditions that enable the use of ΔK as the driving force. Accordingly, tests using lower R values, sensitive to crack closure effects, would be unfeasible.

Further experimental and numerical work is planned to confirm the results obtained in this work.

Acknowledgements

Part of the work shown in the paper has been carried out by Mr. Daniel Gilli, who wrote his master thesis at BAM from November 2019 to June 2020. The contribution of Mr. Gilli is kindly acknowledged.

References

ASTM E647. Standard Test Method for Measurement of Fatigue Crack Growth Rates. American Society for Testing and Materials 2015.

Blasón, S., 2019. Phenomenological approach to probabilistic models of damage accumulation. Application to the analysis and prediction of fatigue crack growth, Doctoral Thesis, University of Oviedo.

Castillo, E., Fernández-Canteli, A., Siegele, D., 2014. Obtaining S-N curves from crack growth curves. An alternative to self-similarity, Int. J. of Fracture 187(1), 159-172.

ISO 12108. Metallic materials - Fatigue testing - Fatigue crack growth method. International Standard 2018.

Johnson, H.H, 1965. Calibrating the electric potential method for studying slow crack growth. Mater Res Stand 5, 442–445.

Kovarik, O., Janca, A., Siegl, J, 2017. Fatigue crack growth rate in miniature specimens using resonance. Int. J. Fat. 102, 252–260.

Kucharczyk, P., Madia, M., Zerbst, U., Schork, B., Gerwien, P., Münstermann, S., 2018. Fracture-mechanics based prediction of the fatigue strength of weldments. Material aspects. Eng. Fract. Mech. 198, 79–102.

Murchio, S., Dallago, M., Zanini, F., Carmignato, S., Zappini, G., Berto, F., Maniglio, D., Benedetti, M., 2021. Additively manufactured Ti–6Al–4V thin struts via laser powder bed fusion: Effect of building orientation on geometrical accuracy and mechanical properties. Journal of the Mechanical Behavior of Biomedical Materials 119.

Newman, J.C., Bigelow, C.A., Shivakumar, K.N., 1993. Three dimensional elastic-plastic finite-element analyses of constraint variations in cracked bodies. Eng. Fract. Mech. 46, 1–13.

Newman, J.C.,Yamada, Y., 2010. Compression precracking methods to generate near-threshold fatigue-crack-growth-rate data. Int. J. Fat. 32, 879-885.

Tabernig B, Pippan R., 2002. Determination of the length dependence of the threshold for the fatigue crack propagation. Eng. Fract. Mech. 69, 899–907.